

DISPLACEMENT OF HEAVY OIL BY CARBON DIOXIDE IN A TUBE

Mohammed Almagrouk A. Ahmad* and Parthasakha Neogi**

Abstract: After using primary and secondary oil recovery methods, about two third of the original oil in place is left behind in the reservoir. Enhanced Oil Recovery (EOR) methods are being used to recover that oil. Carbon dioxide (CO₂) flooding is one of the enhanced oil recovery (EOR) methods that is used to recover the oil. The interest here lies in recovery of heavy crude oil in a capillary tube with a radius of micrometer scale and that oil is displaced by carbon dioxide (CO₂). The dissolution of CO₂ in oil reduces oil viscosity and swells it, making it easier to displace the oil. In immiscible displacement of viscous liquid (heavy crude oil) in a tube by a gas with lower viscosity than the liquid (Carbon dioxide CO₂), a gas bubble moves steadily and leaves behind a thin liquid film of thickness h_x , which is known as the Bretherton problem.

ANSYS® FLUENT software is used to solve the problem of CO₂ displacing heavy oil in a tube. Different velocities, capillary numbers (Ca) and different tube radii are used as an input into ANSYS® FLUENT software to solve different cases. The oil film thickness that left behind (h_x) is reported both without mass transfer and with mass transfer.

The oil film thickness that is left behind, h_x (in the case of fluid mechanics) is decreased when capillary number/bubble velocity is decreased. That was the case for all different radii and different velocity inputs. When there is no mass transfer, the non-dimensional film thickness left behind h_x/R plotted against capillary number fits Bretherton line. With a small capillary number and a radius of 1 μm , the shape of the profile of the CO₂ bubble is a hemisphere and the oil film thickness that is left behind (h_x) is very small. At large capillary number (10^{-1} for $R=1\mu\text{m}$) and small radius (0.1 μm), the profile shape of the CO₂ bubble is pointed. At the center-line of the tube there is no pressure drop in the gas phase nor in the liquid phase, however, most the pressure drop takes place across the interface. Even under mass transfer of CO₂ into oil, bubbles show Bretherton-type behavior. The thickness of thin residual oil film decreases in the presence of mass transfer, leading to an increase in oil recovery. In addition, the oil film thickness that is left behind (h_x) with mass transfer is less than the oil film left behind without mass transfer. Convection in this case opposes the mass transfer and limits how much CO₂ can dissolve in oil.

Keywords: Bretherton problem, carbon dioxide (CO₂) flooding, Enhanced Oil Recovery (EOR), heavy oil.

INTRODUCTION

Primary and Secondary Oil Recovery

Crude petroleum is found in underground reservoirs in sandstone or limestone rock formation. The rock are porous, of pores $\sim 1\mu\text{m}$. In the first stage of oil recovery, the oil is displaced from the reservoir into the wellbore and up to the surface under its own pressure. Initially, the reservoir pressure is considerably higher than the bottomhole pressure inside the wellbore. This high natural differential pressure drives hydrocarbons toward the well and up to surface. However, as the reservoir pressure

declines because of production, so does the pressure differential. To reduce the bottomhole pressure or increase the differential pressure to increase hydrocarbon production, it is necessary to implement an artificial lift system, such as a rod pump, an electrical submersible pump or a gas-lift installation. Production using artificial lift is considered primary recovery. The primary recovery stage reaches its limit either when the reservoir pressure is so low that the production rates are not economical, or when the proportions of gas or water in the production stream are too high. During primary recovery, only a small percentage of the initial hydrocarbons in place are produced.

The second stage of hydrocarbon production during which an external fluid such as brine is injected into the reservoir through injection wells

*Raslanuf Oil and Gas Processing Company, Libya,
m_almabrook85@yahoo.com

**Missouri University of Science and Technology, Department of
Chemical Engineering, MO, USA.

located in rock that has fluid communication with production wells (Craig, 1971). The purpose of secondary recovery is to maintain reservoir pressure and to displace hydrocarbons toward the wellbore. The secondary recovery stage reaches its limit when the injected fluid brine is produced in considerable amounts from the production wells and the production is no longer economical.

One of the limitation of both primary and secondary recovery is about two third of the original oil in place is left behind in the reservoir. Of about 649 billion barrels of oil still in the reservoirs in the United States, 22 billion barrels only are recoverable by conventional means (Aladasani and Baojun, 2010). Thus, the target for enhanced oil recovery processes is a large one, indeed. With these kinds of shortcomings, plus the increasing global demand for oil, producers must look for enhanced methods of oil recovery.

Enhanced Oil Recovery

The development of enhanced oil recovery (EOR) processes has been ongoing since the end of World War II, when operators who owned reservoirs with declining reserves recognized sufficiently quantities of oil remained in the reservoirs after primary and secondary recovery. Research and field activity increased as production from main reservoirs declined, worldwide consumption increased, and discoveries of major new reservoirs become infrequent (Green and Willhite, 1998).

EOR processes can be classified into five categories: mobility-control, chemical, miscible, thermal, and other processes. Each process has its own history, potential, technology, opportunities and obstacles. Various types of EOR methods are described below in brief (Green and Willhite, 1998 and Fig. 1).

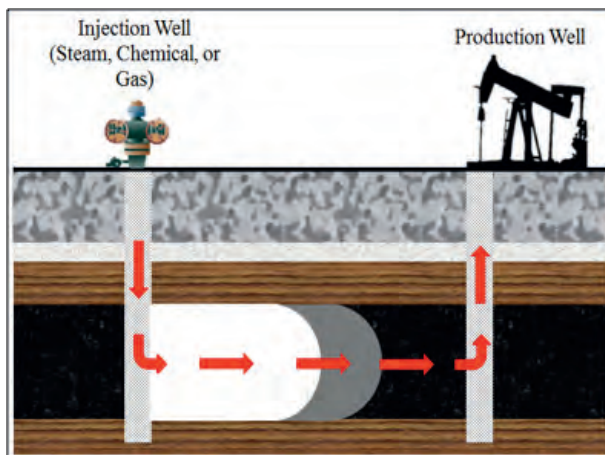


Fig. 1. Enhanced oil recovery methods.

Steam Flooding: This enhanced recovery method is used in heavy-oil reservoirs containing oils where the viscosity is a limiting factor. High temperature steam is generated on the surface then continuously introduced into a reservoir through injection wells. As the steam loses heat to the formation, it condenses into hot water, which, coupled with the continuous supply of steam behind it, provides the drive to move the oil to production wells.

In Situ Combustion: Heat can also be generated in the reservoir by injecting air and burning part of the hydrocarbon (in-situ combustion). Fortunately, only the coke formed from thermal cracking of the most viscous components gets burned. All the lighter components are swept to production by the remaining nitrogen from the injected air. This method is sometimes applied to reservoirs containing oil too viscous or “heavy” to be produced by conventional means. By burning some of the oil in situ (in place), a combustion zone is created that moves through the formation toward production wells.

Alkaline: An enhanced oil recovery technique in which an alkaline chemical such as sodium hydroxide is injected during polymer flooding or water flooding operations. The alkaline chemical reacts with certain types of oils forming surfactants inside the reservoir. Eventually, the surfactants reduce the interfacial tension (IFT) between oil and water and trigger an increase in oil production.

Surfactants: Surfactants can also be injected to reduce the IFT. Good recovery is seen when the IFT reaches ultralow values. By lower IFT gives rise to higher capillary numbers and higher recovery.

Polymers: This has been the most successful chemical EOR case. It enhances the mobility ratio and provides significantly between sweep. However, larger pressures are required. Some loss of polymer during the process is to be expected.

Carbon Dioxide Flood: Carbon dioxide (CO_2) is a common material normally used in the form of a gas and can be sometimes used to enhance the displacement of oil from a reservoir. It can be generated by burning some of the oil produced. It can also be obtained as a by-product from chemical and fertilizer plants, or it can be manufactured or separated from power plant stack gas. The latter case can be coupled to CO_2 sequestration plans (Meyer & Attanasi, 2003; Kovscek, 2002).

Even though CO_2 is not miscible with oil on first contact, when it is forced into a reservoir a miscible front is generated by a gradual transfer of smaller, lighter hydrocarbon molecules from the oil to the CO_2

and the transfer of CO₂ into oil by dissolution. This miscible front is in essence a bank of enriched gas consisting of CO₂ and light hydrocarbons.

This initial CO₂ slug is followed by alternate water and CO₂ injection, with water serving to improve sweep efficiency, that is, make the displacement more stable, and to minimize the amount of CO₂ required for the flood. As reservoir fluids are produced through production wells, the CO₂ reverts to a gaseous state there and provides a “gas lift”. On the surface, the CO₂ can be separated from the produced fluids and may be re-injected helping to reduce the amount of new CO₂ required for the project; thus, the CO₂ can be re-cycled.

The main reason why CO₂ was introduced was that with multiple contacts miscibility could be reached (Hutchinson & Braun, 1961). This is not possible when the oil is heavy oil since heavy oil does not evaporate significantly. However, there are some other benefits in general mentioned earlier. When CO₂ dissolves in oil, it swells the oil, thus squeezing it out from narrow capillaries. In addition, on dissolution of CO₂ in oil, its viscosity decreases up to one order of magnitude (Chung *et al*, 1988). Of course, it is also the least expensive of all EOR processes. As a consequence CO₂ is being tried in oil fields even though CO₂ flooding is the most unstable and requires high pressure.

To quantify CO₂ flooding it is necessary to first know the physical properties of CO₂-oil mixtures. This has been addressed by many investigators and recently (Tran *et al*, 2012) have correlated the data of (Chung *et al*, 1988) using free volume theory. Such data are useful and can be used to study the displacement process.

Instead of simulating the displacement process in a reservoir, we have studied the displacement process in a single cylindrical pore. In the present system as CO₂ displaces heavy oil in a cylindrical capillary, CO₂ dissolves in the oil. This mass transfer process is accompanied by a rise in CO₂ diffusivity in oil, a lowering of viscosity of the oil and increasing in the volume of the oil. Thus, the problem is a moving boundary problem in fluid flow and mass transfer.

Fluid Mechanics

A key factor in brine flooding is the effect of brine-oil surface tension which gives rise to a large retention of oil. One process that has been suggested to recover the remaining oil is CO₂ flooding. Some oil evaporates into the gas phase and some CO₂ dissolves in the oil, leading to miscibility (Hutchinson & Braun,

1961). Miscibility cannot be attained in many heavy oil reservoirs however there are some advantages in using CO₂ flooding. CO₂ swells the oil squeezing it from narrow pores and crevices and it reduces the viscosity of the heavy oil by up to a factor of 10, thus decreases the pressures needed to move the oil. We analyze here the case of CO₂ displacing heavy oil in a single model pore.

When a gas flows into a tube filled with a liquid, it does so in form of a finger (Bretherton, 1961; Miller and Neogi) considered other cases available in literature, a liquid displacing a gas and liquid displacing another immiscible liquid, and summarized the results are shown in [Fig. 2 “A” is the displacing fluid (CO₂ here) and “B” is the displaced fluid (heavy oil)]. Fig. 2 (a) is at equilibrium and the rock is assumed to be preferentially wet by A. As the velocity of displacement is increased, the equilibrium contact angle increases from zero in (a) to a dynamic contact angle of more than 90° (as measured through phase A) in (b) and finally to 180° in (c). At yet higher velocities entrainment takes place as shown in (d).

A number of additional observations are:

- (i) If the rock is preferentially wet by B, then the system starts from equilibrium at (b) and moves down to (c) and (d) with increasing speed.
- (ii) The viscosity ratio is $\chi = \text{viscosity of A} / \text{viscosity of B}$. If χ is near zero (as for a gas displacing a liquid), the transition to (d) occurs at such low velocities that (a)-(c) are practically not

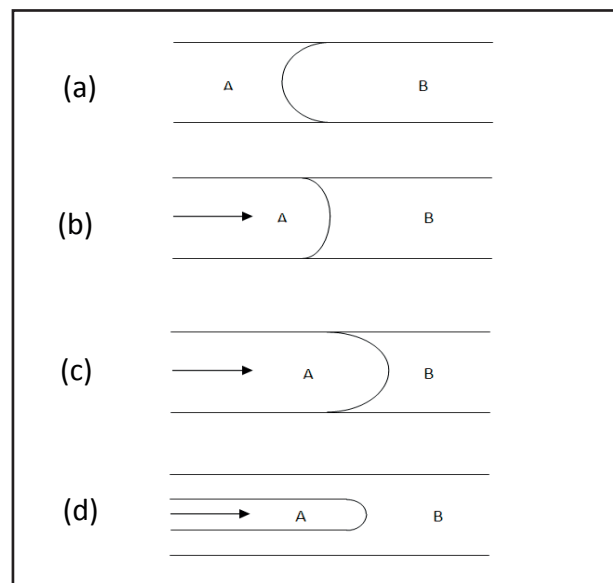


Fig. 2. Fluid B is being displaced by fluid A. (a) shows equilibrium and that B is fully non-wetting. (b) and (c) show the dynamic contact angles α (measured through A) increases with increasing displacement velocity U . Finally in (d) the contact line has entrained.

observed. Conversely, if χ is very high (as for a liquid displacing a gas), the transition occurs at very high velocities.

The problem shown in Fig. 2 (d) is called the Bretherton Problem (Bretherton, 1961) who showed that the thickness of the film of B left behind was determined by hydrodynamics.

The Model: Fig. 3 shows a sketch of the Bretherton problem: a tube with radius R , an inlet pressure p^* drives a CO_2 finger with viscosity μ_1 and density ρ_1 into a fluid (heavy oil) of viscosity μ_2 , density ρ_2 , and surface tension γ . Carbon dioxide enters to the tube at steady speed U and leaves a film of thickness h_∞ behind. It is been assumed that the system remains symmetric about the tube's centerline.

Modeling Setup: The mesh of the computational domain for this problem was created in the preprocessor (GAMBIT 2.4.6). For ease of design, the geometry of the mesh was created with R equal to $1\mu\text{m}$ and L equal to $20\mu\text{m}$ and then it can be scaled up or down in FLUENT. The geometry of the computational domain is shown in (Fig. 4). After creation of the geometry, the boundary types were specified. As illustrated in the figure, the tube has four edges: inlet, outlet, wall and centerline, it is half tube and then it can be axisymmetric in FLUENT to have whole tube. The inlet edge set to be $0.4\mu\text{m}$. After creation of the geometry, the boundary types were specified.

A good mesh should not contain any distorted elements as the CFD analysis can be used only for regular element shapes. The mesh was then exported to FLUENT. The exported mesh was opened in

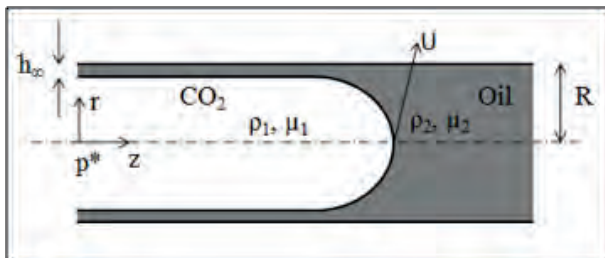


Fig. 3. A sketch of the model problem: a CO_2 finger propagates into a Oil-filled tube.

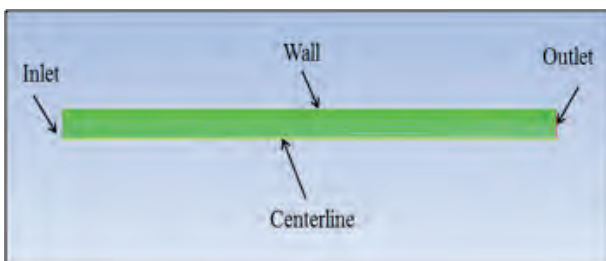


Fig. 4. The mesh and the edges of the tube.

FLUENT 14; there it can be scaled up or down to the required dimensions.

Fluid Flow: Bretherton, 1961 solved this problem approximately. As the interest here is in mass transfer and the changes that occur in the physical properties from it, the problem is solved numerically using FLUENT. Also, inertia is included which has not been taken into account by Bretherton. Bretherton's result is:

$$\frac{h_\infty}{R} = 0.643(3Ca)^{\frac{2}{3}} \quad (1)$$

Where h_∞ is the thickness of the thin film that left behind and the capillary number $Ca = \mu U/\gamma$ where μ is the viscosity of liquid to be displaced and γ is the surface tension. U is the rate of movement of the gas bubble. Bretherton (1961) however, worked with tubes of large radii. In the porous rock formation that contains the crude oil, the lower pore radii drops to $\sim 0.1\mu\text{m}$ and sometimes even lower. Here, the thin films will be greatly influenced by the disjoining pressure (Morrow, 1991). Teletzke *et al* (1988) solved the Bretherton Problem numerically where they included the disjoining pressures. They found that at very low displacement velocities, the effect of disjoining pressure dominates, but at larger velocities Bretherton's fluid mechanical results prevailed. Disjoining pressure has not been included because the interest in this work lies in larger capillary pressures that lead to thicker films that are left behind. Kreutzer *et al* (2005) have presented both experimental and theoretical results for movement at higher velocities. It appears from their profiles that the front of the gas-liquid interface is not a hemisphere but slightly pointed at high velocities.

Formulation for Fluent: The method used by FLUENT to solve free surface problems is the finite volume method (Wesseling, 2001) where the interface is neither sharp nor continuous. Near the interface, we have to have small volume elements otherwise the interface becomes too thick (Fig. 5). The interface is a wide band with varying volume fraction of the gas phase made narrow by decreasing the size of the volume elements.

As a result, whereas width of the elements in z -direction non-dimensionalized by R the tube radius, is kept at 0.1, the ones in r/R progressively shortened. From the centerline the cell size moves outwards in 0.1 nine times. The last section next to the wall is further divided ten times at 0.01 each, and again the last segment is again subdivided ten times with cell sizes of 0.001, and in one case the process repeated once again with a size of 0.0001. The reason for small

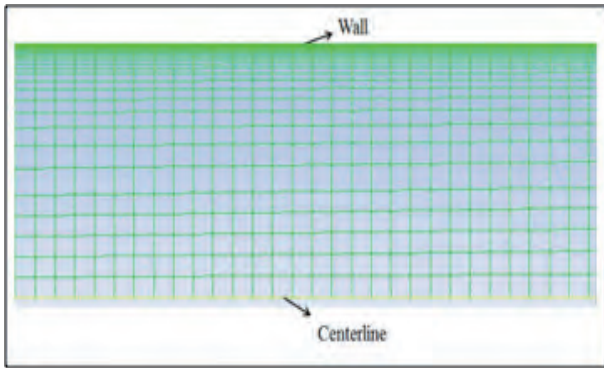


Fig. 5. The size of the volume elements in the mesh which getting smaller near the wall.

volume elements in the r -direction next to the wall is that the interface lies in this region and small elements makes the interface sharp. In addition, h_w/R is a small number and smaller volume elements are needed to calculate this quantity accurately.

Physical Problem Formulation: The problem is treated as an unsteady state problem where CO_2 is introduced at the entrance in a tube of $L/R = 20$, filled with heavy oil. After initial transients, the gas finger moves at a steady rate U into the tube original filled with oil and leaving behind a lubricating layer of thickness h_w . To keep the finger speed U steady, CO_2 is introduced at a constant volumetric flow rate at the entrance. Since this opening is kept smaller than the tube cross-section, U has to be measured separately by locating the nose tip of the finger ($z = z^*$) at different times and taking the slope. This slope is seen to be a constant. U is used to calculate the capillary number Ca .

This approach has a drawback that we cannot plan ahead to come up at a predetermined value of capillary number. We would like to take capillary number from 10^{-8} to 10^{-2} however it takes a very long time to work at small capillary numbers, so work was confined to 10^{-4} to 10^{-1} in keeping with the needs in EOR.

MASS TRANSFER

Carbon dioxide dissolves in oil that is being displaced, but oil is taken to be heavy oil and is assumed not to evaporate into the gas phase. Heavy oil has a specific gravity greater than 0.921 and viscosity greater than 100cp (Tran *et al*, 2012). The important feature is that when CO_2 dissolves in oil and the effect of mass transfer, thermodynamic and transport properties change significantly. Chung *et al* (1988) have reported detail data on the properties of Bartlett crude with and without CO_2 . Tran *et al* (2012) have correlated these properties with free

volume theory. Only one temperature 297.1K (75°F) is considered and their results are:

Henry's law constant:

$$H = 6.544 \times 10^4 \text{ Pa}(CO_2)/(\text{kg}/\text{m}^3)$$

Concentration of CO_2 in the oil at saturation in kg/m^3 : $c_{sat} = p_{CO_2} / H$

and volume fraction:

$$\phi_{sat} = 1.06 \times 10^{-3} p_{CO_2} / H$$

where p_{CO_2} is the gas pressure in the Pa abs.

Swelling factor:

$$SF = \frac{1 - 5.917 \times 10^{-5} p}{1 - \phi}$$

Where p is total pressure in atm.gage

Density in g/cm^3 :

$$\rho = \frac{\phi}{1.06} + \frac{0.94921}{SF}$$

where $\phi = 1.06 \times 10^{-3} c$ and c is the concentration in kg/m^3 .

Viscosity in Pa.s:

$$\ln \mu = \ln(14.8435) + \left[\frac{1}{f + \phi 4.5244 \times 10^{-2}} - 47.89 \right]$$

Free volume fraction without CO_2 is:

$$f = 0.02088 - 5.915 \times 10^{-5} p$$

Diffusivity in m^2/s :

$$D = 5.14 \times 10^{-13} e^{2.659c}$$

The surface tension is (Rojas & Ali, 1988) in mN/m

$$\gamma = 22.626 + 2 \times 10^{-5} p_{CO_2} - 8 \times 10^{-10} p_{CO_2}^2$$

Briefly, they show that oil swells under CO_2 , viscosity decreases by up to one order of magnitude, and the diffusivity increases by an order of magnitude or more.

Consider Fig. 6. If it is assumed that there is no flow in the liquid film left behind, then

$$\pi R^2 \langle v \rangle = \pi (R - h_w)^2 U \tag{2}$$

where $\langle v \rangle$ is the average velocity far from the nose of the bubble. In this region, the flow profile can be assumed to be the parabolic profile of Hagen-Poiseuille's flow. To consider the overall rate of mass transfer, a moving coordinate system can be envisioned.

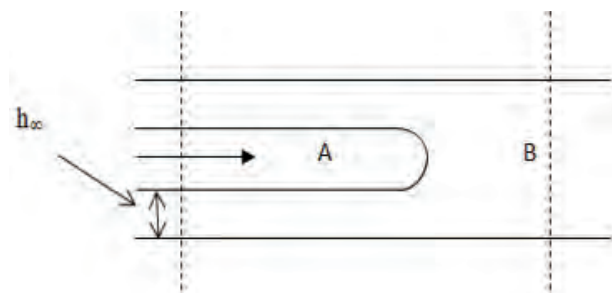


Fig. 6. A model of moving coordinate system.

CO₂ does not reach the station at the front, hence the only place CO₂ leaves the system is with the thin liquid film which can be considered to be saturated and velocity profile has a plug flow backwards at U . Hence the rate of mass transfer in mol/s:

$$M = \pi [R^2 - (R - h_{\infty})^2] U c_{sat} \quad (3)$$

where c_{sat} is the saturation concentration.

The Model

The model for the mass transfer is imposed on the fluid mechanics. Fig. 7 shows a sketch of the problem: a tube with radius R , an inlet pressure p^* drives a CO₂ finger with using coordinates (say affixed to the nose of the meniscus). It is possible to say that for steady displacement, no dissolved CO₂ would have reached the station downstream, all of the liquid upstream would be saturated and if there is zero shear at the liquid-gas interface then the velocity in the liquid would be plug flow at U backwards. Viscosity μ_1 and density ρ_1 into a fluid (heavy oil) of viscosity μ_2 , density ρ_2 , and surface tension γ . Also, it shows the gas volume fraction (ϕ_g) which set to be equal to 1.0 in the gas phase and it equals to 0.0 in liquid phase as it shown in (Fig. 7).

It also shows c_{sat} which is the concentration at the interphase. Carbon dioxide enters the tube at steady speed U and leaves a film of thickness h_{∞} behind.

Finite Volume

As mentioned earlier, when space is discretized into small volume elements, the exact location is of the interface lost. The gas phase is characterized by gas volume fraction $\phi_g = 1.0$. The liquid phase by $\phi_g = 0.0$. Across the interface, ϕ_g takes fractional values. Since the interface has disappeared, it no longer represents a discontinuity or singular surface (Slattery, 1999) hence no jump conditions are needed. In addition, the surface tension is included as a body force (Brackbill *et al*, 1992).

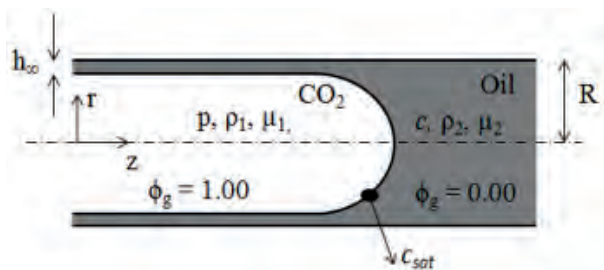


Fig. 7. A sketch of the model problem in presence of mass transfer.

The method used by FLUENT to solve free surface problems is the element of volume or the finite volume method (Wesseling, 2001). It uses a continuous variable ψ , which is 0 in the CO₂ phase and 1 in the oil phase. Since ψ changes continuously, the interface is a wide band which can be made narrow by decreasing the size of the volume elements (Gupta *et al*, 2009). Now, the interface h is located here by locating the element where $\psi \approx 0.5$. FLUENT calculates curvature $2H$ using a method that does not need $h(z)$. It then uses $-2H\gamma$ where γ is the surface tension, which is the Laplace pressure, but it is not used as a surface force in the normal stress balance but it is used as a body force a weight that is proportional to the gradient of ψ (Brackbill *et al*, 1992).

Formulation

The equations of motion, continuity and conservation of species (CO₂) with continuous changes in properties across the interface, are solved to obtain, the velocity v , pressure p and concentration c .

The fluids have been considered to be compressible, the viscosity and diffusivity dependent on the local pressure and concentration of CO₂, and the surface tension at the CO₂-oil interface and solubility of CO₂ there, have been taken to depend on CO₂ pressure. The expressions for the physical properties given above to be included in FLUENT as user define functions (UDF).

There is one exception to this. The outlet pressure in the fluid mechanical problem is set to zero. The net pressure difference is approximately estimated as $2\gamma/R^*$ where $R^* = R - h_{\infty}$, the radius of the gaseous tube. If R^* is approximated as R which is taken to be $1\mu\text{m}$, then the upstream gas pressure is estimated to be about 0.5 atm. To keep the gas pressure down, at least in these calculations the reference viscosity of the heavy oil has been reduced to 1.5 Pa.s and not 14.8435 Pa.s as indicated above. Nevertheless, the flow remains in the low Reynolds number region and explicit algorithm is used.

As mentioned previously, at the entrance ϕ_g is forced to be 1.0 over an inner radius of $0.4\mu\text{m}$ for $1\mu\text{m}$ radius. This forces the gas into the system. At the interface, ϕ_g changes continuously but quickly to zero. Hence, in the algorithm in FLUENT for updating the concentrations is overridden to say that updated c is set to zero, if $\phi_g > 0.7$, $c = c_{sat}$ if $0.4 < \phi_g < 0.7$, but the updating is as is if $\phi_g < 0.4$. That is 0.4 to 0.7 is taken to be the interface.

Further, the knowledge of not only c_{sat} , but also of other quantities like γ , depends on the gas pressure at the interface. It was observed, that when the profile

is Bretherton-type (Fig. 6), the gas pressure at the interface is not significantly different from that at the entrance, that is $p(0,0)$, and this is the value used. Eventually, once the mass transfer iterations are completed, it is necessary to find h_{∞}/R to use in Eq. (3).

To obtain how the concentration of CO_2 varies in oil requires that we solve the conservation of species equation subject to the boundary condition that the concentration is c_{sat} at the gas-liquid interface. Instead of working with concentration c , we multiply the entire conservation of species equation with $v = 1.06 \text{ cm}^3/\text{g}$, the specific volume of CO_2 in oil that was determined earlier for this crude oil (Tran *et al*, 2012). The result is that c is converted to volume fraction ϕ , and with a saturation value of ϕ_{∞} . In FLUENT, we set the inlet concentration to be ϕ_{∞} . After a time step, the new ϕ is reset to ϕ_{∞} but only up to the interface. Thus, the hypothetical concentration of CO_2 “dissolved” in CO_2 is constant at ϕ_{∞} right up to the interface beyond which conventional diffusion equation applies. The concentration on the right exit is set to zero.

RESULTS AND DISCUSSION

Fluid Flow Results

The procedure explained earlier was used to determine the profile shape of the CO_2 bubble in the tube with different tube radii and determine the film thickness that left behind, h_{∞} . It also calculated the pressures, in particular the centerline pressure as a function of axial position z . Note that the outlet pressure is set to zero, hence the pressures are all pressure drops and can also be taken to be the gage pressures. The relationship between capillary number and h_{∞}/R is also noted. In the calculations, three different radii have been used $10\mu\text{m}$, $1\mu\text{m}$, and $0.1\mu\text{m}$ with three different inlet velocities: 0.00168, 0.000168, and 0.0000168m/s. These two quantities were the main inputs to the FLUENT. Based on these inputs, the values of pressure (p), capillary number (Fig. 8). Profiles of the meniscus at $Ca = 1.85 \times 10^{-4}$ and $R = 1\mu\text{m}$ (Ca), and the film thickness that left behind (h_{∞}) were seen to change. Additionally, the shapes of the profiles had different radii and moved with different velocities, when these inputs changed.

The results showed that h_{∞} decreases as capillary number decreases in all cases. Also at large capillary numbers, the profile shape is pointed and for that case h_{∞} cannot be measured because there were steps in the profile which never steadied upstream. Furthermore, small tube radius ($0.1\mu\text{m}$) showed a fingering profile

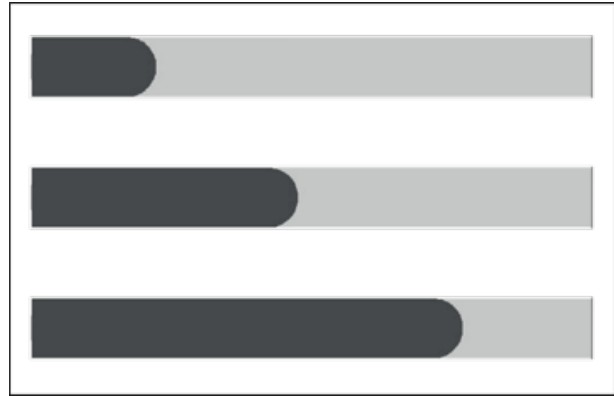


Fig. 8. Profiles of the meniscus at $Ca = 1.85 \times 10^{-4}$ and $R = 1\mu\text{m}$.

even with same value of capillary number that gave good results with larger radius.

The shapes of the profiles for $Ca = 1.85 \times 10^{-4}$ and $R = 1\mu\text{m}$ are shown in (Fig. 8) at different times, that is, the outline of the CO_2 -oil bubble is shown at different positions. The head is a hemisphere, a feature that does not change as long as Ca remains small, and with radius $1\mu\text{m}$ and low capillary number the thickness of the deposited film h_{∞} is very small such that h_{∞} cannot be shown at this scale. The tip of the advancing meniscus is a spherical cap with a radius $\approx R$.

As expected there is practically no pressure drop in the gas phase. Thus, instead of using the pressure of CO_2 at the interface to calculate the surface tension and the solubility, the pressure at the entrance $p(0,0)$ that is, p at $z = 0$ and $r = 0$ is used, since the gas-liquid interface is not so easily located. The outlet pressure has been set to zero and the inlet pressure adjusts itself as the inlet velocity differed. The center-line pressure $p(z,0)$ has been shown in dimensionless form in (Fig. 9) as a function of position z for the same capillary number at different times and with radius equal to $1\mu\text{m}$. Linear pressure drop and Hagen-Poiseuille flow with parabolic profiles were verified in the liquid phase sufficiently far from the head. It is seen that the pressure neither drops significantly in the gas phase, nor in the liquid phase. Most of the pressure drop takes place across the interface.

The Laplace pressure across the hemispherical cap is approximately $2\gamma/R$. Thus, if pressure is non-dimensionalized to $p(z,0)R/\gamma$, it should reach a value slightly in excess of 2. With this result in mind we have plotted the inlet pressure $p(0,0)$ in dimensionless form in (Fig. 10), for three different tube radii, all at a time where the menisci are at z^*/R in the tube, all with inlet velocity equal to 0.000168 m/s, and capillary numbers are all comparable (but not equal). Since the

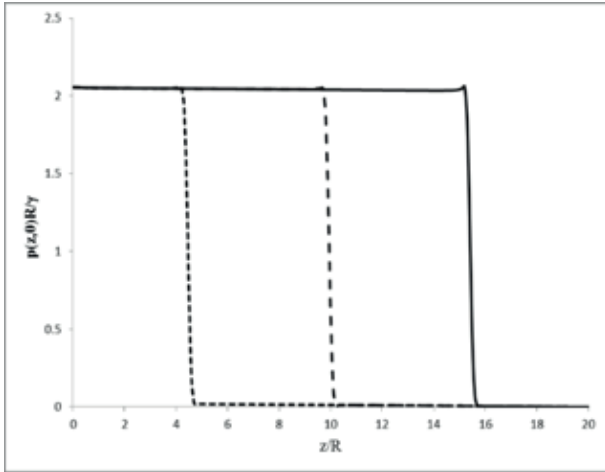


Fig. 9. Non-dimensional Center-line pressure $p(z,0)$ versus position z for same capillary number at different times and $R = 1 \mu\text{m}$.

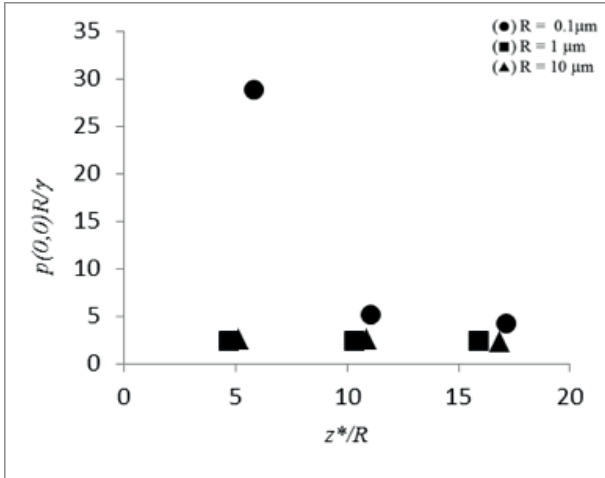


Fig. 10. Non-dimensional inlet pressure $p(0,0)$ for three different tube radii, at a time where the menisci are at z^*/R .

pressure drop across the menisci, contribute to nearly all of the pressure drop, $p(0,0)$, the total pressure drop, is as expected ~ 2 in dimensionless form. This is indeed the case for $R = 1\mu\text{m}$ and $R = 10\mu\text{m}$. However, it is much larger when $R = 0.1\mu\text{m}$. So we looked at how the profile for the gas finger looked for $R = 0.1\mu\text{m}$ which is shown in (Fig. 11).

A much sharper head is seen. Therefore, we conclude that in small tubes, the pressure drops in the gas phase and the liquid phase become quite large as R is decreased below $1\mu\text{m}$. A point is reached where these large forces work to streamline the shape of meniscus such that the total pressure drop is reduced. No change was seen where L/R , which is otherwise = 20 in all cases, was increased to 40. The velocity of the nose was also found to be a constant.

In (Fig. 12), non-dimensional film thickness that left behind h_∞/R has been plotted against capillary number Ca , and they have been compared with

Equation (1). A radius of $1 \mu\text{m}$ was used in FLUENT with three different velocities which were represented three different capillary numbers: $1e-2$, $1e-3$, and $1e-4$. The squares stand for h_∞/R versus Ca , and the straight line represented Bretherton equation. The figure showed that the numerically calculated results were almost as same as Bretherton results. It also verified that film thickness that left behind h_∞ was decreasing when capillary number decreased.

It has been mentioned above that the ratio between the length and the radius of the tube (L/R) was = 20, with this ratio and for capillary number of 10^{-1} the h_∞ cannot be measured because there were a steps in the profile. So, the ratio was increased to 40 to see if there would be any difference (Fig. 13). However, the graph showed the same results and there was no difference. So far, only the fluid mechanics have been considered. next, the effects of mass transfer will be discussed.

Mass Transfer Results

The results of mass transfer calculations have been plotted in (Figs. 14 & 15), against capillary number

Ca and Peclet number $Pe = \frac{U2R}{D}$ respectively,



Fig. 11: Profile for gas finger with $R = 0.1 \mu\text{m}$.

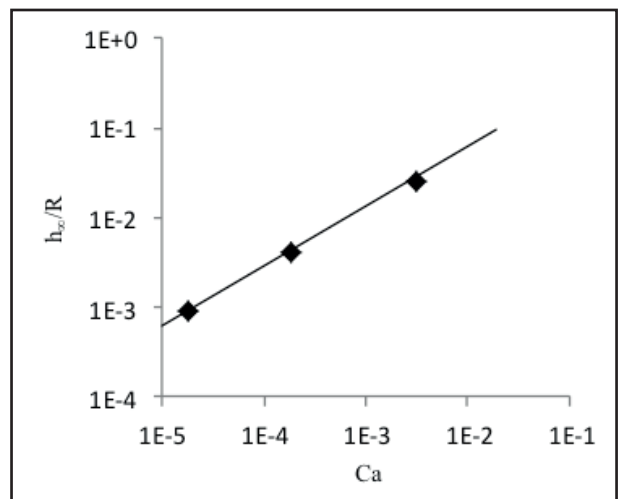


Fig.12. Non-dimensional film thickness that left behind h_∞/R plotted against capillary number Ca and compare them with Equation (1).



Fig.13. Profile of capillary number equal to 10^{-1} and with 40 L/R ratio.

where \bar{D} is an average diffusivity, averaged from p_{sat} to zero. The diffusivity is:

The average is given by:

$$\bar{D} = \frac{5.14 \times 10^{-13}}{4.063 \times 10^{-5}} (e^{(4.063 \times 10^{-5} p_{sat})} - 1) \quad (4)$$

In both cases, Bretherton equation, Equation (1) is used as a basis for comparison. From Equation (3), it is possible to show that for small values of h_{∞}/R , the dimensionless mass transfer rate is:

$$\frac{M}{\pi R^2 c_{sat} U} = 1 - (1 - h_{\infty}/R)^2 \approx 2h_{\infty}/R \quad (5)$$

Thus, the dimensionless mass transfer rate is proportional to h_{∞}/R . If we consider the special case where the concentration of dissolved CO_2 is very low throughout, then the fluid flow will not change and the calculated h_{∞}/R and Ca pair will fall on the Bretherton line. Thus, the Bretherton equation provides a basis for comparison.

Non-dimensional film thickness that left behind h_{∞}/R has been plotted against capillary number Ca , in (Fig. 14), and they have been compared with Equation (1) in presence of mass transfer. Two different radii $10\mu\text{m}$ and $1\mu\text{m}$ were used with four different velocities. The straight line represented Bretherton equation, the squares stand for $10\mu\text{m}$ and the triangle stand for $1\mu\text{m}$. The figure verified that film thickness that left behind h_{∞} in presence of mass transfer was decreasing when the capillary number decreased. What is observed in (Figs. 14 & 15) is that convection decreases the mass transfer, quite contrary to intuition. However, the mass transfer is seen to decrease with convection from a low value and it is mainly in (Fig. 15), that a limit is observed.

That is, reaches the lowest possible value and does not change anymore with increasing Pe . On returning to (Fig. 14), it is seen that at large capillary numbers both cases of two tube radii, lead to the same asymptote that parallels Bretherton's case. Also, it showed that the oil left behind (h_{∞}) with mass transfer is less than the oil left behind without mass transfer.

The explanation of the negative impact of convection lies in the fact that in the front of the bubble, convection is in the direction opposite to the direction of diffusion. Increasing convection also squeezes the domain through which the CO_2 penetrates the oil at the tip of bubble. In fact, we were unable to draw the contour plots of CO_2 in oil in a meaningful way due to the very large compaction. However, the decrease in mass transferred is not without limits.

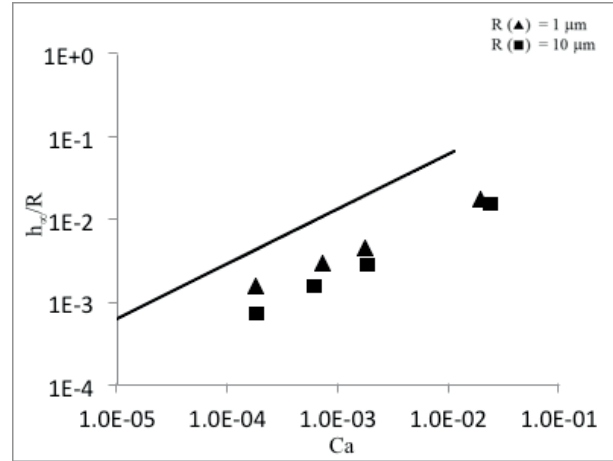


Fig. 14. Non-dimensional film thickness that left behind h_{∞}/R plotted against capillary number Ca in presence of mass transfer, with $R = 10$ and $1\mu\text{m}$, and compare them with Equation (1).

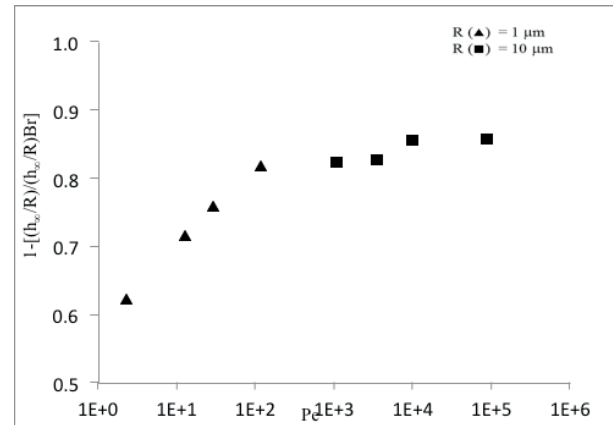


Fig. 15. Dimensionless film thickness as a function of Peclet number Pe . Mass transfer (dissolution CO_2 in oil) falls when the trend rises.

More squeezing increases the concentration gradient and diffusion flux, reaching limits in a manner similar to concentration polarization.

CONCLUSIONS

In fluid mechanics case, the oil film thickness that left behind, h_{∞} is decreasing when capillary number/bubble velocity decreases. That was the case for all different radii and different velocity inputs. The h_{∞}/R versus Ca and Bretherton line are almost identical. At large capillary number (10^{-1} for $R = 1\mu\text{m}$) and small radius ($0.1\mu\text{m}$), the profile shape of the CO_2 bubble is pointed.

Even under mass transfer of CO_2 into oil, the profile shape of the CO_2 bubbles show Bretherton-type profiles. The oil film thickness left behind (h_{∞}) with mass transfer is less than the oil left behind without mass transfer. The mass transfer decreases with

increasing convection as the convection is opposed to the direction of diffusion and the preferred direction of mass transfer. The fluid flow alters considerably from Bretherton type at small capillary radius and at large velocities, in same manner.

ACKNOWLEDGMENT

Author wishes to thank his company Raslanuf Oil and Gas Processing for its help and support. Also, he would like to express his sincere thanks to his adviser Dr. Parthasakha Neogi, Truynh Tran (his research mate), and the Missouri University of Science and Technology for the constant guidance, opportunities, support and encouragement they have given to complete this study.

REFERENCES

- Aladasani, A. and Baojun, B. (2010). Recent Developments and Updated Screening Criteria of Enhanced Oil Recovery Techniques. *SPE 130726*: 24p.
- Brackbill, J. U.; Kolthe, D. B. and Zemach, C. (1992). A Continuum Method for Modeling Surface Tension. *J. Comp. Phys.*, **100**: 335-354.
- Bretherton, F. P. (1961). The Motion of Long Bubbles in Tubes. *J. Fluid Mech.*, **10**: 166-188.
- Chung, F. T. H.; Jones, R. A. and Nguyen, H. T. (1988). Measurements and Correlations of Physical Properties of CO₂/Heavy-Crude-Oil Mixtures. *SPE Res. Eng.*, **3**: 821p.
- Craig, F. F. Jr. (1971). The Reservoir Engineering Aspects of Waterflooding. *Monograph Series, SPE*, Richardson, Texas 3.
- Green, D. W. and Willhite, G. P. (1998). Enhanced Oil Recovery. *Soc. Pet. Eng.*, **V. 6**: 545p.
- Gupta, R.; Flecture, D. F. and Haynes, B. S. (2009). On the CFD Modeling of Taylor Flow in Microchannels. *Chem. Eng. Sci.*, **64(12)**: 2941-2950.
- Hutchinson Jr., C. A. and Braun, P. H. (1961). Phase Relations of Miscible Displacement in Oil Recovery. *AICHE. J.* **7**: 64p.
- Kovscek, A. R. (2002). Screening Criteria for CO₂ Storage in Oil Reservoirs. *Pet. Sci. Tech.*, **20**: 841p.
- Kreutzer, M. T.; Kaptejin, F.; Moulijn, J. B.; Klein, C. R. and Heiszwolf, J. J. (2005). Inertial and Interfacial Effects on Pressure Drop of Taylor Flow in Capillaries. *AICHE. J.*, **51**: 2428-2440.
- Meyer, R. F. and Attanasi, E. D. (2003). Heavy Oil and Natural Bitumen-Strategic Petroleum Resources. (<http://pubs.usgs.gov/fs/fs070-03/fs070-03.html>, accessed 07/03/12).
- Miller, C. A. and Neogi, P. (2008). Interfacial Phenomena, Static and Dynamic Aspects, 2nd ed., Boca Raton, FL: CRC Press: 421p.
- Morrow, N. R. (1991). Interfacial Phenomena in Oil Recovery. New York, NY; Marcel Dekker: 446p.
- Rojas, G. A. and Ali, S. M. F. (1988). Dynamics of Subcritical CO₂/Brine Floods for Heavy Oil Recovery. *SPE Res. Eng.*, **3**: 35-44.
- Slattery, J. C. (1999). Advanced Transport Phenomena, Cambridge University Press: 709p.
- Teletzke, G. F.; Davis, H. T. and Scriven, L. E. (1988). Wetting Hydrodynamics., *Revue Phys. Appl.*, **23**: 989-1007.
- Tran, T.; Neogi, P. and Bai, B. (2012). Free Volume Estimates of Transport and Thermodynamic Properties of Heavy Oils with CO₂. *Chem. Eng. Sci.*, **V. 80**: 100-108.
- Wesseling, P. (2001). Principles of Computational Fluid Dynamics, Springer: 644p.